Universitat
de les Illes Balears

Synchronization in a Neural Mass Model

Ana Alonso Castillo

Director: Claudio R. Mirasso (IFISC)

Master's Thesis

Master's degree in Physics of Complex Systems

Universitat de les Illes Balears

September 2017

Abstract

It has been shown in simple neuronal systems, conformed by two excitatory neurons unidirectionally (sender-receiver) connected, that the receiver neuron can anticipate the sender spiking if an inhibitory neuron is connected bidirectionally to the receiver. Later, the same behavior was reproduced using neural networks although was computationally very costly. In this work we study synchronization in the Neural Mass model proposed by M. Breakspear, 2003 and observe that, under certain conditions, it does also display anticipated synchronization while being computationally more efficient than neural networks simulations.

Acknowledgements

I would like to express my gratitude to:

- Claudio, for his kindness and guidance and for the opportunity of learning in such an inspiring environment. For letting me glimpse what research is about and helping me face new questions and problems.

- The professors of the master and the IFISC. It has been such an interesting and fruitful year. Plenty of work, but with a huge reward and a great feeling at the end.

- To my flatmates and colleagues of the master. They made the work and the free time in Palma awesome and funny.

- To the special person on the other side of the phone with whom I can share my weaknesses and achievements.

- Finally, to my parents that believed in me and made this possible with their economic support. Most importantly, thanks to the education they gave me and the values they taught me.

Dedication

Als meus pares, que m'han ensenyat el significat de l'esforç.

"Neurons giveth and neurons taketh away."

- *Abhijit Naskar, The Film Testament*

Contents

List of Tables

List of Figures

Chapter 1

Introduction

1.1 Motivation and State of the Art

Unveiling the dynamics and functions of the brain is a goal for neuroscientists, physicists and mathematicians among many other scientists. Nowadays, computational neuroscience is in its most active moment thanks to the large amount of data we are able to record and analyze. This enables us to develop, rectify and discard models but, while we can describe a single neuron well enough, understanding a large group of them interacting is still a very challenging problem.

One can start studying a group of neurons from an structural point of view [1][2], and end up describing the physical connections of the brain using graphs and complex networks theory [3]. Or from a functional point of view, analyze the rich activity they display such as synchronization [4][5], neuronal avalanches [6] and learning [7][8] within the theoretical framework of dynamical systems and statistical physics.

These phenomena, although believed to be very important in the brain, are common in a variety of systems, for example in lasers [9][10], sand-piles [11] and adaptive systems [12] and can be described by a growing field of physics called complex systems. Complex systems provide mathematical and computational tools to understand emergent phenomena arising from interactions and the dynamics of the constituents.

Although there is no clear delimitation for what complex systems can or cannot describe, the brain is probably one of the most complex systems we can imagine. It is conformed with billions of neurons in the microscopic level, following electric and chemical rules that no one is directing and although they can resemble very chaotic from outside, it is believed they end up giving rise to reasoning and consciousness, phenomena of completely different nature. We are indeed, very far from answering which is the link between cognitive performance and the brain components but we can focus in understanding isolated behaviors first.

An example of these isolated behaviors is the synchronization between different regions of the brain. This phenomena is related to information processing [13] and has been proposed as a mechanism for justifying the high velocity of the brain when identifying images [16]. Other studies also proved that synchronization in the brain is related to attention [14][15] and short-term memory. The speed of brain's information processing seems to rely then, in some mechanism we cannot understand solely by transmission of pulses and diffusion of chemicals, but as a result of the interaction of neurons.

Not only that but recently [17] it as experimentally shown that the brain can exhibit also anticipated synchronization (AS).

AS is a counterintuitive phenomena. Regular synchronization between two systems occurs in a way that the information goes from the master or sender to the slave or the receiver. The master is excited first and the excitation is propagated due to some coupling term until it reaches the slave system that with the perturbation gets also excited. Then talking of neurons, the Master one fires first and the Slave fires afterwards. However this is not the only case, although information always flows from Master to Slave, in AS regime the Slave system advances the sender and fires first.

AS has been studied previously in lasers [18][19] and in neural systems where simulations where carried out using individual neurons in [20] or neural networks [17]. However, this is not the only approach we can give to this problem. Other methods have been proposed to simulate the activity of a group of neurons that, we believe, also reproduce this data with much less computational cost.

The activity of the neurons we want to reproduce corresponds to data recorded during electroencephalogram (EEG) experiment, and thus are measures of the evoked potential in the scalp. The evoked potential recorded is then caused by a whole cortical column which is a much larger system than a neural network of a hundreds of elements. This amount of neurons are hardly difficult to simulate from a microscopic point of view and then, one is forced to take some kind of considerations and approximations in order to find a realistic description for this phenomenon.

We can describe those cortical columns as previously done in [21] with Neural Mass (NM) models. This allows us to consider each of this brain columns as a NM that is in general traits, a system with a common potential shared for all the constituents, sometimes interpreted as a huge neuron. Neural Mass Models are then very useful because they reduce largely the dimensionality of the system while still displaying a behavior very similar to the one obtained in the experiments and showing a very rich activity. Further investigations in this direction have been published recently as for example [22][23].

Following this direction, it is interesting to continue testing NM models to see how realistic they are and if they can exhibit also the same behavior found in more detailed simulations as for example the ones using neural networks. By doing so we can understand better these models and prove them to be a meaningful and useful representation of a cortical column or otherwise be aware of which limitations they have and review with more detail the simplifications made to derive them.

It is a good step forward to understand what kind of mechanisms we are able to describe using NM models as those are computationally efficient and can help simulate experiments and conceive new problems we would not be able to afford otherwise. Some of the open questions in this field, that could be approached by following this direction of study are in creating new and more involved activity models with spatial structure and large physical connections or searching for more sophisticated phenomena as the reproduction of the activity in different regions of the brain or either short or long term memory.

1.2 Outline

Our objective will be to simulate a NM using a model proposed by Larter and Breakspear based in Morris-Lecar [24] equations to describe the evolution in time of the membrane potential of a cortical column. Next, we will study the NM dynamics by itself and couple it with another NM of similar characteristics reproducing the synchronized behavior previously founded in [25]. Finally, we will try to find anticipated synchronization, a phenomena shown also in neural networks simulations and in experiments.

Chapter 2

Background Theory

To better understand what a NM model consist of, let us first introduce the biological phenomenon we try to reproduce. Starting from the microscopic level, we will explain the relevant mechanisms that allow neurons to pulsate.

2.1 Biological Description

The brain is the main organ of the nervous system and it is conformed by a network of neurons supported by glial cells. It is believed that the dominant role in processing all the information is done by neurons and that glia cells are in charge of protecting neurons and ensure they are isolated and well provided of nutrients and oxygen. Recent studies found that glia cells could be also participants in some more involved tasks, for example: creating connections between neurons and breathing. However, his behavior is still limited and disregarded when considering electric circuits and modeling neurons activity.

Focusing on neurons, when they are in the resting state, it exists a characteristic difference of potential between the cell and the environment, $V_{rest} \approx -70mV$, and the membrane is said to be polarized. This is due to the existence of ions such as Na^+, K^+ and Ca^{2+} and Cl^-, that are distributed as seen in Fig 2.1 creating electrochemical gradients in the membrane.

Then, one can find in the surface of the neuron an accumulation of positive charge, due to the concentration of Cl^- and Na^+, while K^+ and negative proteins are accumulated on the inside reproducing the scheme of a typical capacitor.

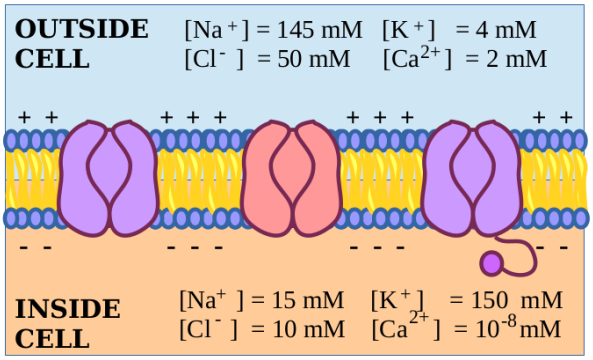

Figure 2.1: Graphical description of the ion concentration in the cellular medium.

Those electrochemical gradients are maintained by Sodium-Potassium pumps, but the neuron also has other gates to allow ions cross the membrane under different circumstances in order to generate spikes. We can find voltage-gated channels, that allow ions to cross the membrane when the neuron reaches an specific membrane potential. Neurons also have, ligand-gated channels, that open when a specific neurotransmitter attaches to its receptor and the less common, mechanically-gated channels that open in response to the physical stretching of the membrane.

If a neuron is perturbed but its potential is not larger than $V_{th} \approx -55mV$ the neuron decays to its resting state again. However if the perturbation goes beyond the V_{th} the neuron produces a spike and then returns to the resting state.

The process of spiking is the following, see Fig 2.2. When a local part of the neurons is sufficiently perturbed, (0) the neuron excites and an electrical change occurs, (1) sodium and calcium channels open and the ions enter inside the neuron, this changes the potential of the cell making it positive and the neuron is depolarized. Before reaching the maximum potential (2), potassium channels open, allowing K^+ to flow outside the neuron. This process is called repolarization and reverts the effect of the perturbation decreasing the neuron potential again. Once in (3) the voltage keeps decreasing until Sodium-Potassium pumps recover the V_{rest}. Other ions have a less important role and are considered part of the leakage current.

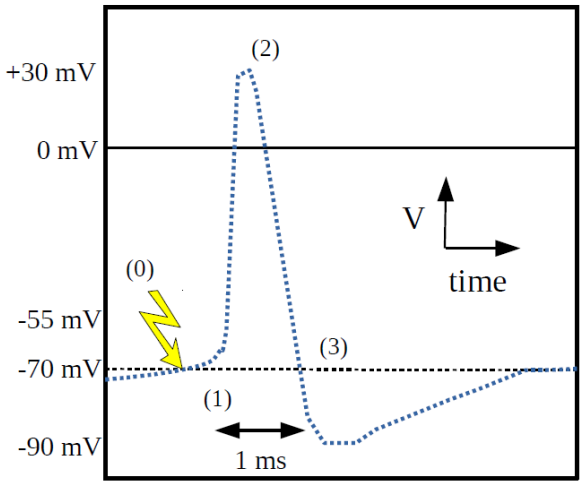

Figure 2.2: Graphical description of the action potential of the neuron.

This spike is local but it is transmitted all along the axon of the neuron. The membrane of the neuron is full of those ion channels, and once a region changes polarization the ones nearby are affected and also change polarization, this ends up in a cascade effect propagating the spike through the neuron and to other neurons at the end.

The way neurons transmit the signal to other neurons is by a process called synapses. There are two types of synapses, electrical and chemical. Electrical synapses are less common and are bidirectional, they are much faster than chemical synapses because they can pass ion currents directly from one neuron to the other through a gap junction. However, although electrical synapses are fast and useful are not the most common because they excite directly every neuron. This could be useful for specific situations, such as heart beats but they could be dangerous and end up saturating regions of the brain if more common. Chemical synapses instead, do not transmit the impulse directly but with the help of neurotransmitters, this makes them more precise and selective and help in not saturating the brain. This kind of synapses are slower and unidirectional.

The mechanism underlying chemical synapses is the following. When the impulse arrives at the tip of the axon, near the synaptic cleft, the presynaptic neuron releases the neurotransmitters. These neurotransmitters are captured by the ligand-gated channels of the postsynaptic neuron and open them allowing the flux of ion currents in the following neuron.

There are different types of neurons with different functions associated to each one. The ones we will focus on are:

- Excitatory neurons, those neurons are typically of Pyramidal type and can have long range connections. They release neurotransmitters such as glutamate or dopamine that attach to ligand-gated channels of NMDA and AMPA type. They produce a positive change of voltage to the neuron they are connected to.
- Inhibitory neurons, in contrast to excitatory ones come in a variety of shapes and morphologies as discovered by Ramon y Cajal. They release GABA neurotransmitters that attach to ion channels $GABA_A$ and $GABA_B$, that allow Cl^- and K^+ ion currents to pass through them. Those neurons produce a negative change of potential to the ones they are connected.
- Interneurons represent 20-30% of the neurons and are in charge of connecting neurons of different type. They can be divided in two groups, local and relay ones. The local ones have short range connections and process small amounts of information while the relay ones have long range connections in order to link different regions of the brain. Interneurons can be either excitatory or inhibitory although are mainly inhibitory.

Other types of neurons show excitatory and inhibitory behavior as they release both types of neurotransmitters. There are hundreds of different types of neurons that can be categorized depending on its structure or functionality.

2.2 Microscopic Description

From a mathematical point of view, neurons are dynamical systems and several models have been proposed for characterizing its behavior. Starting from the simplest integrate and fire model [26], where the evolution of the membrane potential of a neuron is described by a circuit composed of a capacitor and a resistance in parallel, to more elaborated ones such as Hodgkin and Huxley [27] or FitzHugh-Nagumo [28].

In this project we are going to focus in one in particular, the Morris-Lecar [24]. This model is a combination of the last two mentioned and is based on a biological description of the ionic currents that take place in the neuron. In order to arrive to its final expression, the model takes into account the characteristic slow scale of the potassium current and neglects the sodium current. The model does not considers lag between the potential of the membrane and the opening/closure of ion gates. The voltage then varies as

$$\begin{aligned} \frac{dV}{dt} &= -g_{Ca} m_\infty (V - V_{Ca}) - g_K w (V - V_K) - g_L (V - V_L) + I_{ext} \\ \frac{dW}{dt} &= \phi \frac{w_\infty - w}{\tau_\infty} \end{aligned} \tag{2.1}$$

where V is the membrane potential and W is the recovery variable that describes the relaxation process of protein channels between conducting and non-conducting states. The probabilities of having calcium and potassium channels open, m_∞ and w_∞ are given by,

$$\begin{aligned} m_\infty(V) &= 0.5\left[1 + tanh\left(\frac{V - V_1}{V_2}\right)\right] \\ w_\infty(V) &= 0.5\left[1 + tanh\left(\frac{V - V_3}{V_4}\right)\right] \end{aligned} \tag{2.2}$$

and are derived from the assumption that, in equilibrium, are partitioned according to a Boltzmann distribution.

The time constant for the K^+ channel relaxation is given by

$$\tau_\infty = \tau_0 sech\left(\frac{V - V_3}{2V_4}\right) \tag{2.3}$$

where τ_0 is the time scale of the recovery process. This parameter can widely vary as a function of the cell and the temperature. Description for the resting parameters can be found in the appendix, Table 1. Parameters are adimensional, a derivation of the nondimensionalisation of those equations can be found in [29]

Neurons are dynamical systems that are quiescent or active as a function of the applied external

intensity, as an excitable system. In the case of the Morris-Lecar equations, neurons start to fire for sufficiently large values of the intensity, and as a function of the values of the parameters its threshold intensity varies. Not only that but the way the neurons start spiking also varies as a function of the parameter values. Then one can differentiate between two categories.

The first one is called Class-I excitability and is related to Homoclinic and Saddle Node on Invariant Circle (SNIC) bifurcations. When the system undergoes one of these bifurcations, it starts to fire, at the intensity threshold, at an arbitrary low frequency. In the case of the Homoclinic bifurcation, this is due to a logarithmic divergence of the period, $\sim ln(I)$, while in the case of the SNIC bifurcation the period grows like $\sim I^{-1/2}$.

The case of the Class-II excitability is different. The system starts to activate at a given frequency. In general, this is due to a Hopf bifurcation, where the amplitude of the oscillations grows like $\sim I^{-1/2}$, if more specifically, the bifurcation is a Subcritical Hopf, one may observe a fold of cycles that leads to some bistable behavior.

Usual values for the parameters are shown in the appendix, Table 1. The model can display different behavior as it can reproduce both Class-I and Class-II excitability by changing the parameters (see also Table 2 in the appendix). Examples of both cases and the corresponding traces are plotted in Fig 2.3.

The Morris-Lecar model assumes that the dynamics of a neuron can be expressed with a two dimensional system. Although this model is not able to reproduce some behaviors such as bursting oscillations and chaos, that can only be seen in 3-dimensional systems, reproduces quite well other behaviors associated to neurons.

In order to simulate a whole network of neurons, in the range of hundreds to thousands components, one has to assign a proportion of each type of neuron as well as the percentage of connections between neurons. This depends on the region of the brain one wants to model. In the cortex is usually assumed that excitatory neurons are 80% of the total and the inhibitory ones represent the 20%. They are randomly connected, with a probability of connection around 10-20%.

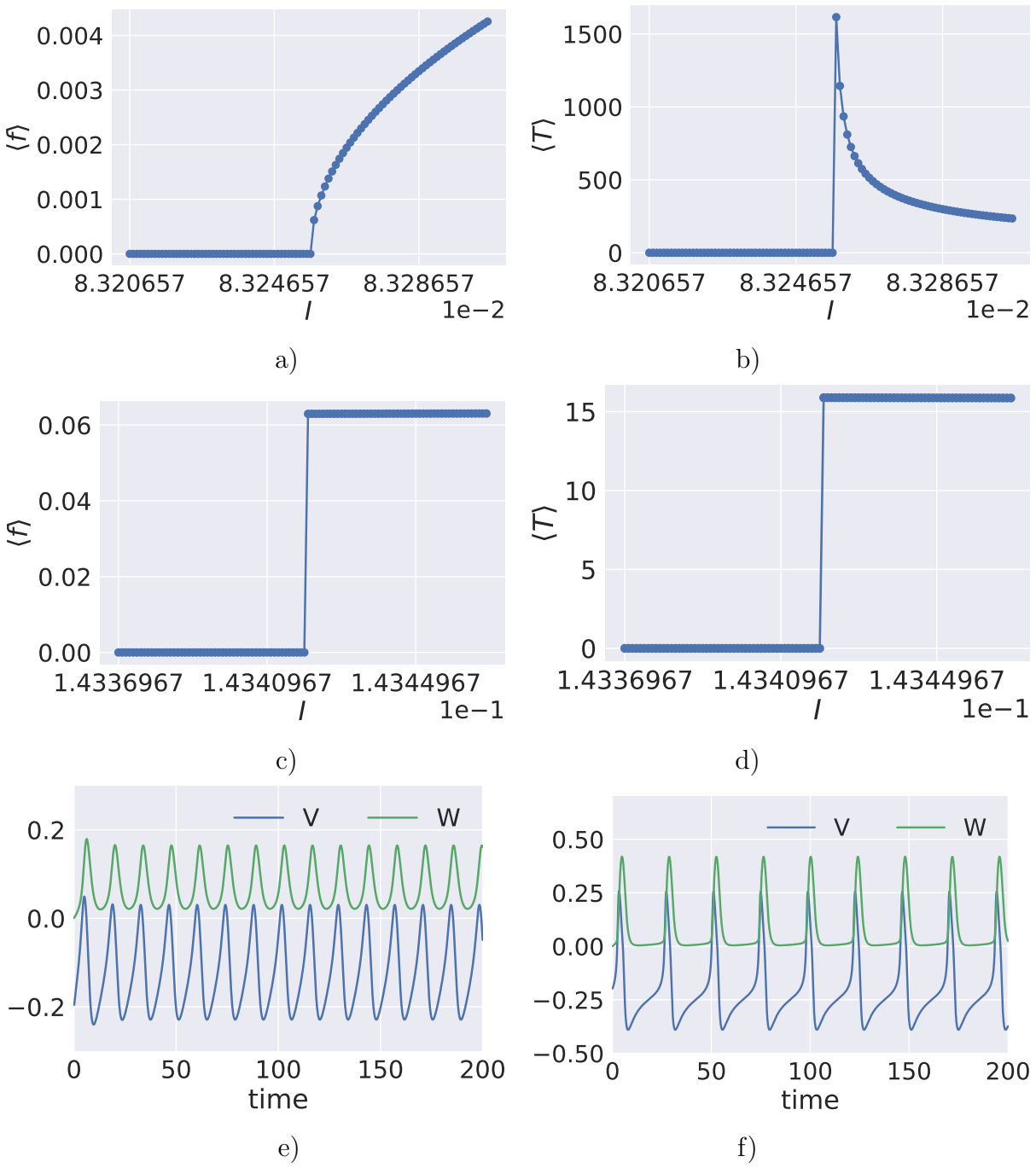

Figure 2.3: Plots of the frequency displayed by the Morris-Lecar model versus the intensity applied for Class-I and Class-II excitability parameters. We can differentiate in (a) and (b) a continuous tendency to zero for the frequency and a divergence of the period. While, one can observe a very sharp discontinuity for the Class-II excitability around $I \approx 0.14341$ for (c) and (d). Example of trajectories displayed by the model for Class-I excitable system in (e) and Class-II in (f)

Connections between neurons should be mediated by synapsis. As we have discussed in the previous section, synapsis can be fast or slow and are simulated by first order differential equation. This would be characterized by the probability, P_{pre}, of releasing the neurotransmitter

of the presynaptic neuron and the probability, P_{post}, of capturing the neurotransmitter at the postsynaptic neuron, so the total probability of the process is $P = P_{pre}P_{post}$. This can be written in the following way

$$\frac{dP(t)}{dt} = \alpha(1 - P(t)) - \beta P(t) \tag{2.4}$$

Here, P, is the fraction of open receptors. α is the opening rate of the channel and β determines the closing rate of the channel. Usually, α, is assumed to depend on the concentration of neurotransmitters as seen in [30] but β is considered constant.

Overall this is computationally very costly. As there are five equations describing the state of each neuron, and two more accounting for each synapse in the network. The number of operations escalates quickly and the size of the network due to our computational resources could be hardly larger than 10000 neurons. This is still far from representative of our brain.

This is why other approximations have been proposed in the literature in order to overcome this problem. Those are mesoscopic models that are based on mean-field and Laplacian approximations and reproduce a region of the brain using a reduced number of variables.

2.3 Mesoscopic Description

One can find two types of mesoscopic representations of a group of neurons. Convolution models that are mathematically based models [31] and conductance-based models, that describe biological meaningful mechanisms [25].

Anatomically, a NM represents a cortical column. When talking about a NM we will refer to cylindrical cortical columns that are in the scale of $10^{-3} - 10^{-2}m$ and that contains thousands of neurons. These columns have six different layers occupied each by a different type of neurons, as shown in sketch of Fig. 2.4. The first layer, the external one, is the molecular layer which is conformed only by input axons and contains low density of neurons. Second and third

layers are more dense and mainly consist of excitatory pyramidal neurons. The fourth layer is where the inputs of the thalamus arrives, and then has a higher concentration of inhibitory interneurons. Layer five and six are again mainly conformed by excitatory pyramidal neurons. Inhibitory interneurons connect with other layers of the cortex, that are also linked between them creating complex loops. A simplification of these connections is usually modeled as a dynamical system conformed with excitatory pyramidal cells and inhibitory cells, where these last ones provide a feedback loop to the first [32].

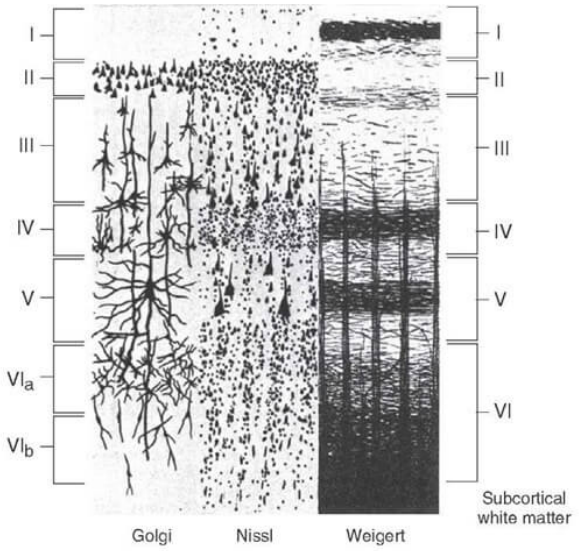

Figure 2.4: Picture of a cortical column using different methodologies. Golgi captures a small percentage of neurons, Nissl reveals the shape of the cell body and Weigert stains the myelinated axons. Picture is taken from Clark (1959) *The Anatomy of the nervous System. Its function and development.* in [33].

The activity of pyramidal cells is what is measured in Electroencephalogram (EEG) experiments [34]. This is because pyramidal cells have longer axons and are perpendicular to the scalp. However, interneurons, both inhibitory and excitatory, do not have a prominent role in the signal recorded.

The model proposed by M. Breakspear et al in [25] was based in previous neuronal model of Morris-Lecar [24] extended by R. Larter et al in [35] in order to simulate epileptic seizures in the hippocampus.

Each NM is conformed by a large number of neurons, each described in our case by a Morris-Lecar system of equations (2.1), so each neuron has three variables characterizing its state,

$x = \{V, W, I\} \in \mathcal{R}^N$. To solve this in a computational efficient way, it has been proposed in [36], [37] and [38] to describe the dynamics of each neuron using a Langevin equation where $f(x)$ stands for the Morris-Lecar equations describing the dynamics of the neurons plus some random fluctuations following stochastic differential equations such as,

$$dx = f(x)dt + \sigma dw \tag{2.5}$$

where σ controls the amplitude of the fluctuations and $w(t)$ is a standard Wiener process. With this we obtain a set of equations that can be integrated to obtain the dynamics of the ensemble of neurons. All neurons would populate the phase-space with a density $q(x, t)$ that would evolve in time until reaching an equilibrium or stationary state. The dynamics of the density of states can be described by a Fokker-Planck equation,

$$\dot{q} = -\nabla f q + \nabla D \nabla q = -\sum_{i=1}^{N} \frac{\partial (f_i q)}{\partial x_i} + \sum_{i,j=1}^{N} \left(\frac{\partial}{\partial x_i} D_{i,j} \frac{\partial}{\partial x_j} \right) q \tag{2.6}$$

where $D(\sigma) = \sigma^2/2$ is a diffusion tensor. Here, one has to assume a statistical description of the population given by the distribution of neuronal states. An important approximation involved in this representation of a group of neurons is that intensity inputs to each neuron are considered uncorrelated and the individual spiking rate is substituted with an ensemble average time-dependent population activity.

However, the problem of large dimensionality still remains, as this method does not specify how the ensemble density of states, $q(x, t)$, should be integrated. This can be handled binning phase-space, but doing this could make our system again too complicated to solve it computationally. One can overcome this problem assuming a fixed form of the density, the simplest form is taking a delta-function or point mass, this is when we obtain a NM model.

2.3.1 Mean-Field Interaction Between Excitatory and Inhibitory Neurons

If we consider each type of neuron to be independent, in our case the excitatory pyramidal cells and the inhibitory interneurons, then $m = 2$ as is the number of different populations in the neural mass and the ensemble density becomes,

$$q(x) \approx \Pi_{i=1}^{m=2} q(x_i). \tag{2.7}$$

This assumption is rather strong, as implies that there are no correlations between the dynamics of different type of neurons. With the aim of solving this statement, it has been proposed that only the mean activity of one ensemble, μ, impairs an effect on the other one and vice-versa, so the dynamics are now described by, $f(x, \mu)$, where $\mu_j = \mu(q(x_i))$. This is still a severe assumption, but not as strong as the last one, because now we are only disregarding the effects of fluctuations between different sorts of neurons.

The strength with which the mean activity influences the different type of neurons, can be understood as the coupling between them or the effective connectivity. So we obtain that the mean membrane potential of all pyramidal excitatory neurons behave following the equation in (2.1) as

$$\begin{aligned} \frac{dV(t)}{dt} = &- \{g_{Ca} + r_{NMDA} a_{ee} Q_V(t)\} m_{Ca} (V(t) - V_{Ca}) \\ &- \{g_{Na} m_{Na} + a_{ee} Q_V(t)\} (V(t) - V_{Na}) \\ &- g_K W(t) (V(t) - V_K) - g_L (V(t) - V_L) \\ &- a_{ie} Z(t) Q_Z(t) + a_{ne} I_{ext} \end{aligned} \tag{2.8}$$

where other important variables are the fraction of active potassium ion channels W and the fraction of open channels of other ions that are involved in the process m_{ion}. Q_V and Q_Z are the mean firing rate of the neural mass and are described by the following equations

$$\begin{aligned}
\frac{dW(t)}{dt} &= \frac{\phi(m_{_K} - W(t))}{\tau_{_W}} \\
m_{_{ion}} &= 0.5\left[1 + tanh\left(\frac{V() - T_{_{ion}}}{\delta_{_{ion}}}\right)\right] \\
Q_{_V}(t) &= 0.5\left[1 + tanh\left(\frac{V(t) - V_T}{\delta_V}\right)\right] \\
Q_{_Z}(t) &= 0.5\left[1 + tanh\left(\frac{Z(t) - Z_T}{\delta_Z}\right)\right]
\end{aligned} \tag{2.9}$$

The parameters value and its description can be found in the appendix, Table 3.

Population of inhibitory neurons has been proposed to be modeled in [25] as,

$$\frac{dZ(t)}{dt} = b(a_{_{ni}} I^0_{_{ext}} + a_{_{ei}} V(t) Q_{_V}(t)) \tag{2.10}$$

In order to find a realistic description of the biological system we also assume, in the same way we did for the Morris-Lecar model, that $m_{_{ion}}$ obeys a sigmoid like function, equation (2.9). The probability of having the ion channel open is supposed to be more or less instantaneous depending on the $\delta_{_{ion}}$ parameter. The same happens for the mean firing rate of the NM that introduces some variability in the firing threshold and is described with the same type of function.

This model is biophysically meaningful and the parameters correspond to biological quantities. This represents a great advantage as models of synchronized systems are sometimes done with simple coupled oscillators that are not realistic enough, in the sense that it is hard to know if the regime one is checking corresponds directly to some physically meaningful state of the brain.

Chapter 3

Exploring Larter-Breakspear's Model

The Larter-Breakspear model has a wide variety of regimes. Here we report some of them found for different sets of parameters. Values for those parameters are fixed following Table 3 in the appendix and varied as described next. In Fig 3.1 and 3.2 we show some examples of the mentioned regimes.

As in the case of the Morris-Lecar, we have used dimensionless set of parameters in the simulations. The equations were integrated without noise, using the Euler Method and an integration step of $h = 10^{-5}$. We started all computations with uniformly distributed random initial conditions.

For values of $\delta_v < 0.55$ the system has one stable fixed point. So from the initial conditions, the NM depolarizes and settles onto a resting state. This behavior corresponds to Fig 3.1 (a) and (b).

If we fix $0.55 < \delta_v < 0.59$, the system goes through period-doubling bifurcations exhibiting some characteristic behaviors. For example the limit cycle attractor shown in Fig 3.1 (c) and (d) and a period-9 orbit as shown in Fig 3.2 (a) and (b). This could be understood, biologically speaking, as burstings.

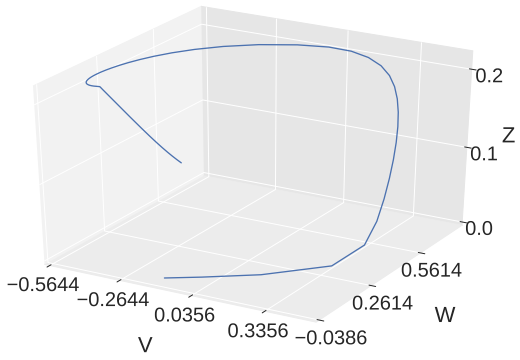

a)

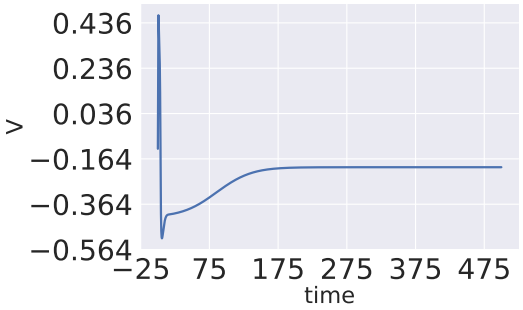

b)

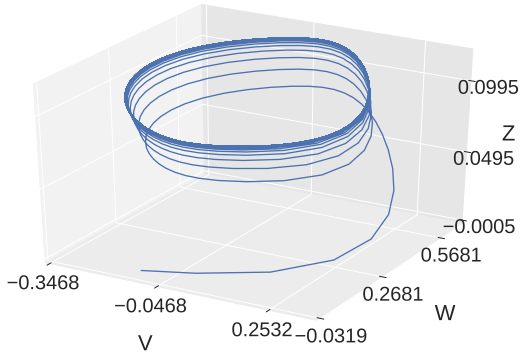

c)

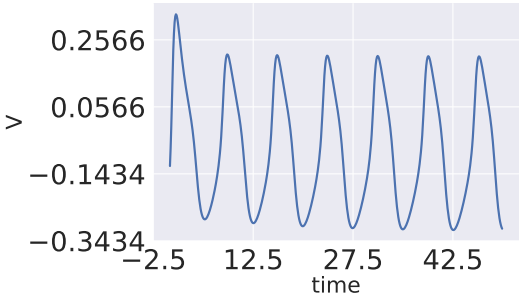

d)

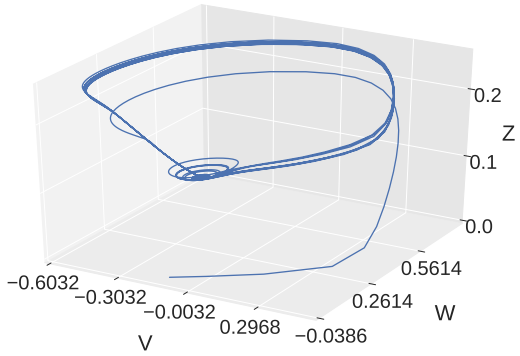

e)

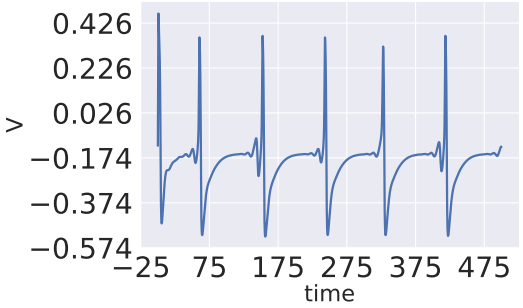

f)

Figure 3.1: This figure shows different behaviors of the Larter-Breakspear's Model corresponding to different parameters mentioned in this section. In Fig. (a), (c) and (d) we can see the a 3D representation of the trajectories. The space is defined by the three variables of the model V, W and Z. In Fig (b), (d) and (e) we have plotted traces of excitatory neurons measured over time, $V(t)$.

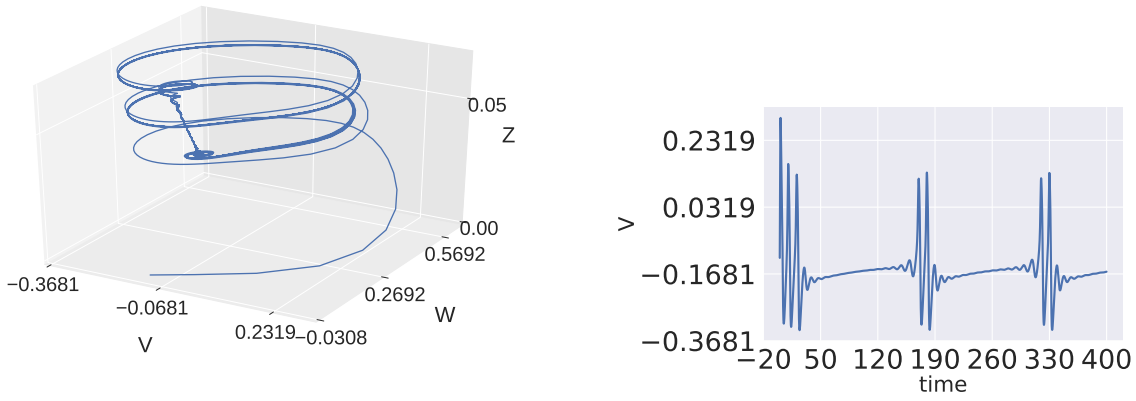

a) b)

Figure 3.2: For values of δ_V near 0.6 and $a_{ee} = 0.5$, $a_{ie} = 0.5$, $g_{Na} = 0.0$, $I_{ext} = 0.165$, $a_{ni} = 0.1$, $V_T = 0.5$ the system shows a 9-period limit cycle attractor.

Those previously mentioned period-doubling bifurcations can result in a chaotic behavior for $\delta_V > 0.59$. An example is shown in Fig 3.1 (e) and (f), with $\delta_V = 0.65$. Although reported to be chaotic, this system is highly structured [25]. This allows us, in the absence of noise, to find meaningful measures for certain characteristic magnitudes.

To determine the type of excitability for the parameters of Table 3 and $\delta_V = 0.65$, we computed the frequency versus intensity plot, shown in Fig 3.3. The result obtained has a discontinuity in the frequency for values of I above a threshold and recalls a Class-II excitability. However, one must be cautious before assuming this, as a small discontinuity in the frequency could be due to numerical errors or approximations. The amplitude dependence with the intensity is shown in Fig 3.3 (c) where it jumps from zero to a fixed value. There is an interesting regime near the discontinuity where one can see that the model may go to a fixed point or to a limit cycle, depending on the initial conditions. Thus, displaying bistable behavior.

Now, instead of using random initial conditions for each measure we make a continuation plot, with one curve starting from large values of I_{ext} and another from low ones. This will help us to see more clearly the bistable region of the diagram responsible of hysteresis, Fig 3.3 (d), which is a characteristic of a Subcritical Hopf Bifurcation. Is the fact that the bistable region is small that makes the system display this Class-II excitability.

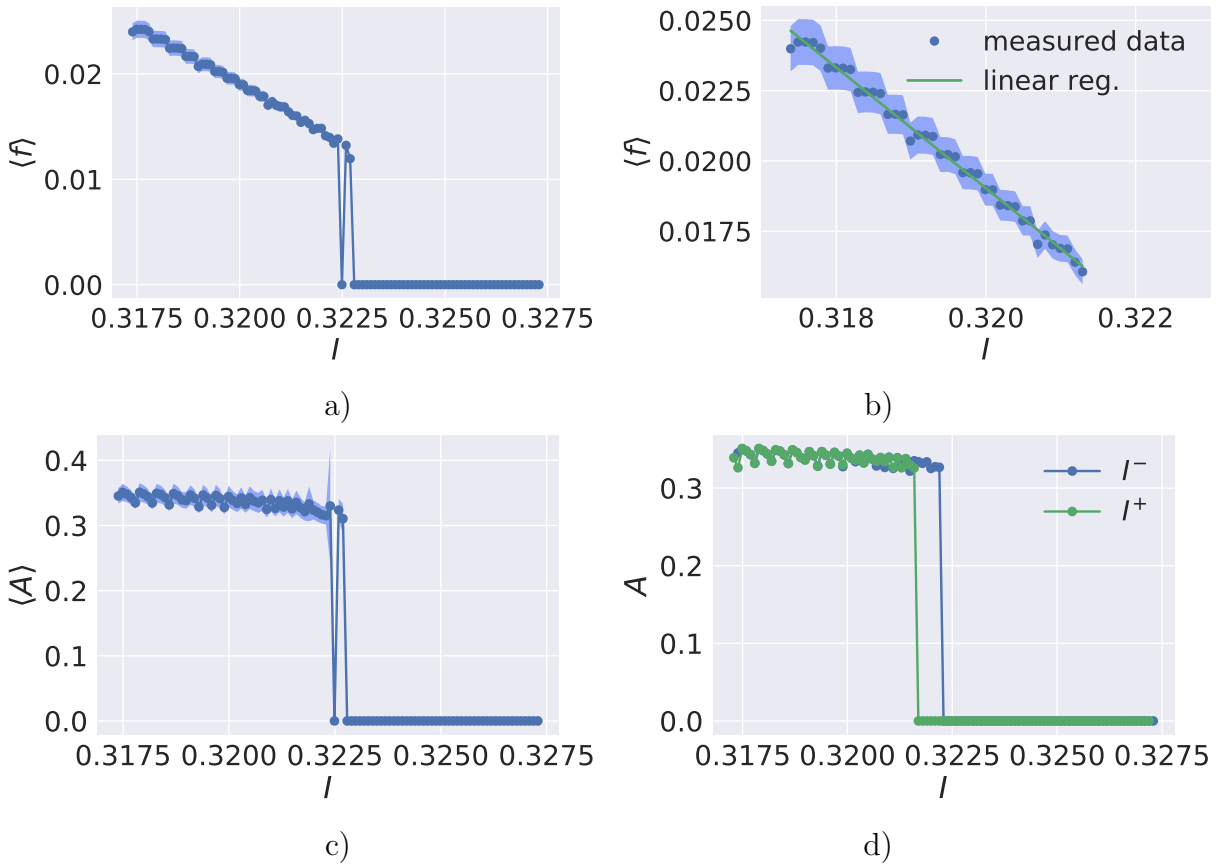

Figure 3.3: Plots of the frequency displayed by the model versus intensity applied for $g_{Ca} = 1.1$, in (a).The linear regression is plotted in (b) and the dependence of the amplitude in (c). The histeresis typical of a Subcritical Hopf bifurcation is shown in (d). Averages are made over 10 trials. I^- corresponds to the continuation plot starting from low values and I^+ to the continuation plot starting from high values of the I_{ext}.

We fitted the parameters of the linear regression of the mean frequency vs. the injected current, $y = mx + b$. For the case of $g_{Ca} = 1.1$, a good linear dependence of the frequency with the intensity is found.

$$m = -2.14 \pm 0.06 \qquad b = 0.71 \pm 0.02 \qquad r = 0.991,$$

If we increase the calcium conductance and fix it to $g_{Ca} = 2.1$, as done for the simple Morris-Lecar model, one can see a clear Class-I excitable system, Fig 3.4. We found a logarithmic dependence, characteristic of a Homoclinic Bifurcation, the parameters of the fitted linear regression in this case take values

$$m = 235.6 \pm 0.3 \qquad b = -254 \pm 1 \qquad r = 0.999.$$

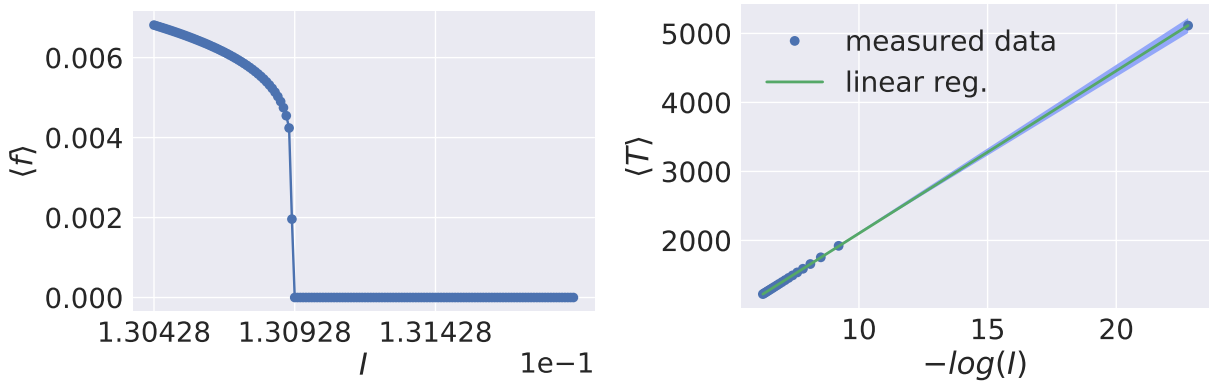

a) b)

Figure 3.4: Plots of the frequency versus intensity applied using $g_{Ca} = 2.1$ in (a) and its linear regression in (b). Averages are realized over 10 trials.

$Q_V(t)$ explicitly depends only on the voltage of the excitatory neurons and the parameters δ_V and V_T. So it is also interesting to see how the firing frequency of the NM varies as a function of other parameters of the model. Here, in order to understand better the behavior of the equations we vary the strength of the internal connections between different type of neurons. The results obtained for different values of the connectivity constants can be seen in Fig 3.5 and 3.6 and are the result of 50 averaged measures in equidistant values of the parameters $a_{ee}, a_{ei}, a_{ie}, a_{ne}$ and a_{ni}.

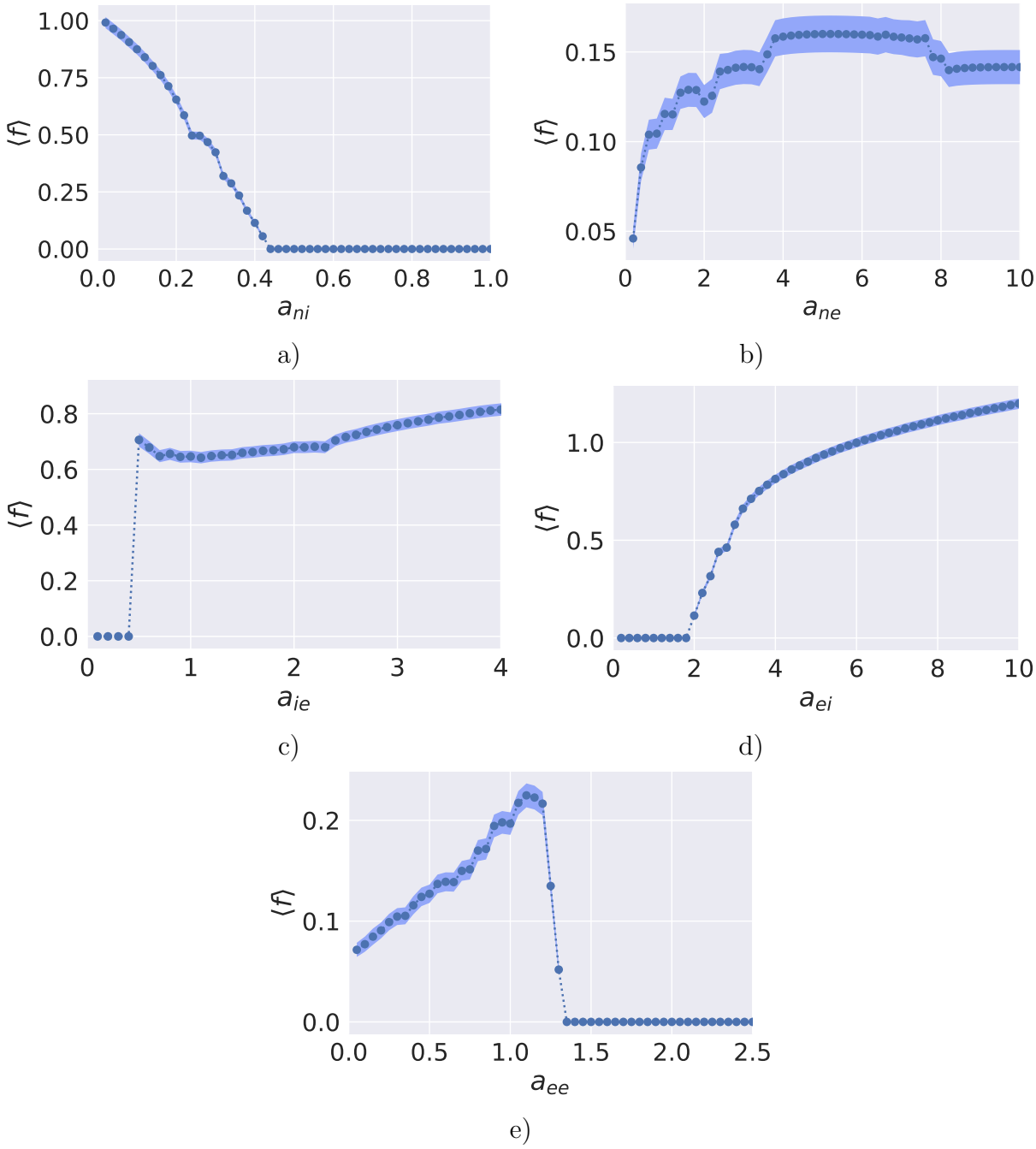

Figure 3.5: Average frequency corresponding to NM traces for different values of the internal connectivity constants. Other parameters were fixed corresponding to the Class-II excitability regime. Values were calculated over 50 trials for equidistant values of the control variable.

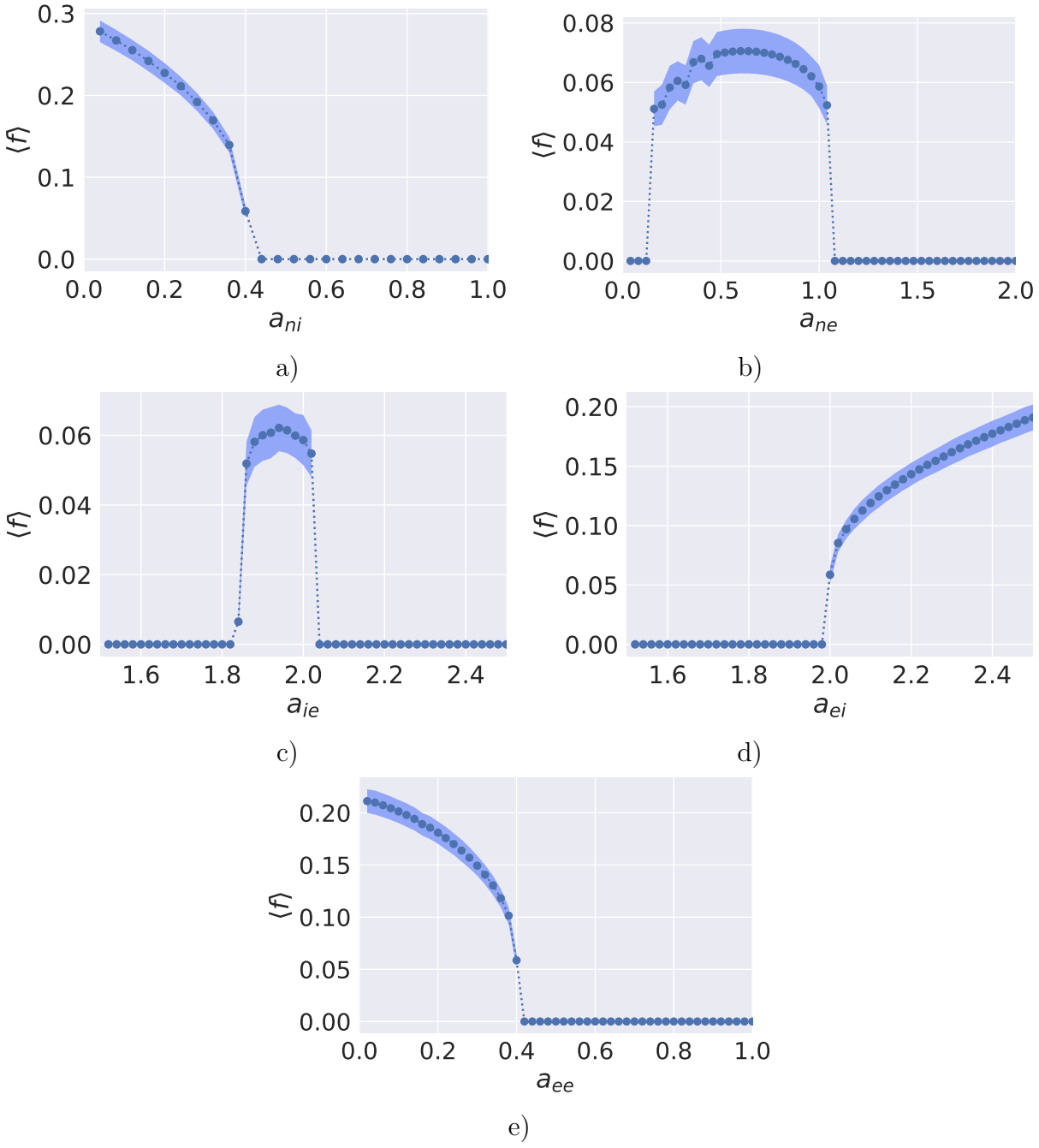

Figure 3.6: Average frequency corresponding to NM traces for different values of the internal connectivity constants. Other parameters were fixed corresponding to the Homoclinic bifurcation. Values were calculated over 50 trials for equidistant values of the control variable.

Chapter 4

Synchronization

The study of synchronization goes back to the 17th century, where Huygens gave a description for two weakly coupled pendulum clocks. Since the studies of Huygens, synchronization has been reported in systems of diverse nature, applauses, fireflies and even cardiorespiratory rhythms. But one must be careful in what is or is not synchronization. Specially, should not be mistaken for resonant effects. When we talk about synchronization we will consider it as a complex dynamical process that depends on the ability of each system to adapt. Meaning that there is not enough information in a solely measure of the system given one set of initial conditions but we need to check the behavior it has for different initial conditions to see if synchronization is a property of the system or just a fortuity.

In order to talk about synchronization one should have two oscillating systems, not necessarily periodic and neither with the same characteristic frequency. The systems should be weakly coupled and as a consequence, accommodate one to each other. Even if the oscillators have their own rhythms at the beginning, they adjust and end up sharing the same frequency after the coupling. The keymark, in order to find synchronization is to obtain a constant phase shift between the two coupled systems. Mathematically this condition can be written as $|t^M - t^S| = K$ where, in our neuronal example, t^M is the time the master neuron spikes and t^S is the time the slave neuron spikes. If this condition is fulfilled we can say the system is in a phase-locking regime.

Huygens studied, as a function of the initial conditions of the pendulum, different regimes obtaining in-phase synchronization or anti-phase synchronization. Nowadays, a lot of different casuistics have been found to cause different types of synchronization as for example: complete synchronization, generalized synchronization, lag synchronization or anticipated synchronization and more recent studies aim to develop a general theory for all these concepts [39].

Specifically, some neurons behave as relaxation oscillators and do not usually describe sinusoidal waveforms. They use to show an accumulate-and-fire behavior. For example in the case a pulse of current is injected into the cell, if this is sufficiently large the neuron reaches the potential threshold and depolarizes quickly. In the case that the input of current is constant the spikes are usually generated at a constant rate.

It is our aim in this section to find synchronization for different parameter values of the NM. Starting from the simplest unidirectionally coupled system. In this kind of systems the pulse is transmitted from the master NM to the slave NM, as seen in Fig. 4.1. More involved examples could incorporate bidirectional coupling and delayed coupling; they will be also studied later.

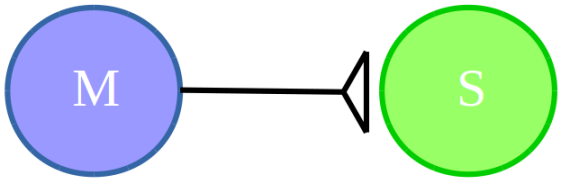

Figure 4.1: Scheme of a unidirectional excitatory coupling between two different NM. M stands for the Master and S for the slave NM.

4.1 Synchronization in Larter & Breakspear Model

To couple N NMs we used a unidirectionally link based in competitive excitatory synapses between pyramidal cells, with a constant $C = \Sigma_j C_{ji}$ as shown in [25] that can take values in the range between $C = [0, 1]$.

$$
\begin{aligned}
\frac{dV^i(t)}{dt} =& -(g_{Ca} + (1-C)r_{NMDA}a_{ee}Q_V^i(t) + Cr_{NMDA}a_{ee}\langle Q_V^j(t)\rangle)m_{Ca}(V^i(t) - V_{Ca}) \\
& -(g_{Na}m_{Na} + (1-C)a_{ee}Q_V^i(t) + Ca_{ee}\langle Q_V^j(t)\rangle)(V^i(t) - V_{Na}) \\
& -g_K W^i(t)(V^i(t) - V_K) - g_L(V^i(t) - V_L) + a_{ie}Z^i(t)Q_Z^i + a_{ne}I_{ext} \qquad (4.1) \\
\frac{dW^i(t)}{dt} =& \frac{\phi(m_K - W^i(t))}{\tau_W} \\
\frac{dZ^i(t)}{dt} =& b(a_{ni}I_{ext}^0 + a_{ei}V(t)Q_V^i(t))
\end{aligned}
$$

Where $i = 1, .., N$ is the index associated to one NM and $\langle Q_V^j \rangle$ is the average firing rate of the NM coupled to i. The other two equations corresponding to inhibitory neurons, Z and potassium channels, W, remain the same as in [25]. This is because the coupling does not affect directly inhibitory neurons; it has been reported in [40] that long-range connections are mainly excitatory.

Considering now the configuration presented in Fig. 4.1, when $i = 1$, $C = C_{21} = 0$ and when $i = 2$, $C = C_{12}$. We will refer from now to the master NM as $i = 1$ and the slave NM as $i = 2$.

Long-range coupling, between NM is more sparse or weak than between neurons in the same NM so we considered $C < a_{ee}$ and $C < a_{ie}$.

An example of synchronization in NM is shown in Fig. 4.2 (a) and (b). The period between spikes as a function of the coupling strength C is depicted in Fig 4.2 (c). The results show that the system displays synchronized behavior for values of the coupling between $0.1 < C < 0.2$. One can see a centered distribution for $C > 0.1$. For $C \geq 0.2$ the average value of the period does not change. The parameters used in these cases are the ones near the Class-II excitability.

Until now, we have shown synchronization between identical NMs but this is not a necessary condition in order to observe this phenomenon. One can couple columns with small variations in the parameters. Staying near the Class-II excitable regime, we still observe that NMs end, after a transient, in the phase-locking regime. Thus, we have shown that synchronization is robust against small changes in δ_V and also to internal connectivity constants.

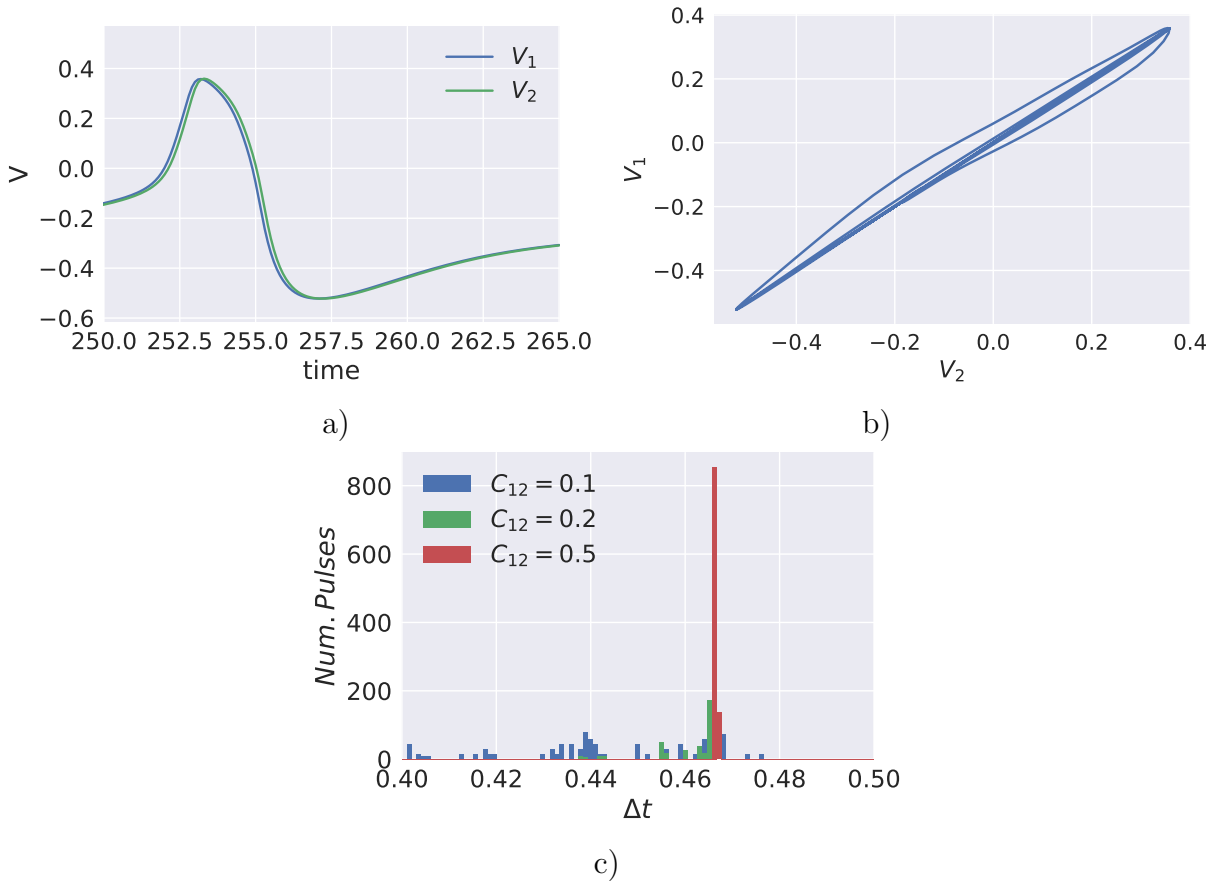

Figure 4.2: Results of synchronized NMs using Class-II excitability parameter values. Traces of synchronized NMs are shown in (a) for $C = 0.13$. The voltages of the Master and the Slave NMs are plotted in (b) where after a transient, V_1 and V_2 are correlated with $C_{12} = 0.13$. As said before, V_1 stands for the master membrane potential and V_2 stands for the slave membrane potential. Synchronization is indicated by a line of 45^o. In (c) we shown the time distribution between spikes for different values of the coupling strength C.

We next check if synchronization is stable for parameter values near the Homoclinic Bifurcation. However, this is not the case as one can see in the histogram representation of the interspike time distribution shown in Fig. 4.3 (a) and (b).

For $C < 0.2$ the system does not display a centered distribution, an example for $C = 0.1$ displaying phase drift is shown in Fig 4.3 (c). In the case of a larger coupling strength, $0.2 < C < 0.3$ the system is in a phase locked regime, however, the receiver system produces two spikes for each one sended by the master. 4.3 (d). For $C > 0.5$, the system reproduces a very sparse histogram corresponding again to non phase-locking between traces. An example of a characteristic trace for a value of C in this range is plotted in Fig 4.3 (d). Not even with a high coupling strength, $C \sim 0.9$, synchronization seems to be stable, leading after a transient

to unstable trajectories.

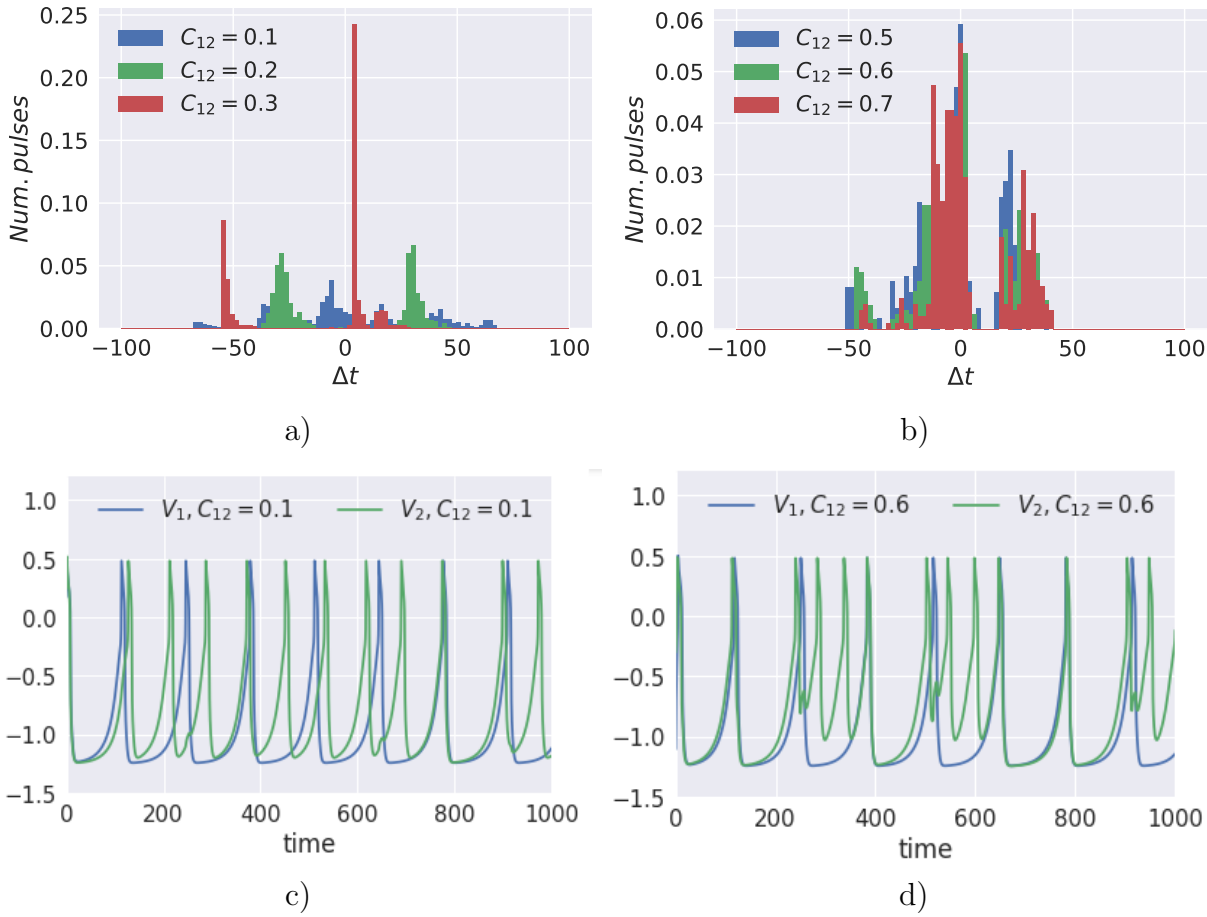

Figure 4.3: Results obtained using Class-I excitability parameter values. In (a) and (b) one can see the time distribution between spikes for different values of the coupling strength. Traces displaying phase-drift are shown in (c) for $C = 0.1$ and in (d) for $C = 0.6$.

4.2 Discussion

Previous studies in neural networks have approached synchronization relating it with the excitability class of the system. However the complete understanding of the mechanisms that allow synchronization is still a debate today.

Measuring the Phase Response Curve (PRC) has been proposed as a useful tool for approaching this problem. PRC relates individual dynamics with the dynamics of a coupled system. This is done by analyzing the effect that an external small current pulse applied to the neuron has on it.

After perturbing a periodic neuron, with period T, its next spike moves forward, firing at $T - \Delta t$, or backward in time, $T + \Delta t$. As a function of the moment we perturb it delay or anticipation happens. So one can plot $PRC(t) = t_{spike}^{free} - t_{spike}^{perturbed}$. Where t_{spike}^{free} is the time at which the neuron fires without perturbation and $t_{spike}^{perturbed}$ is the time at which fires after being perturbed.

The PRC is assumed to be positive if the spike after the perturbation is advanced and negative if it is delayed. According to the PRC, neurons can be of Type-I or Type-II. Type-I PRC neurons only have positive PRC while Type-II PRC neurons have positive and negative PRC. As shown in Fig. 4.4, Morris-Lecar neurons can have Type-I or Type-II PRC.

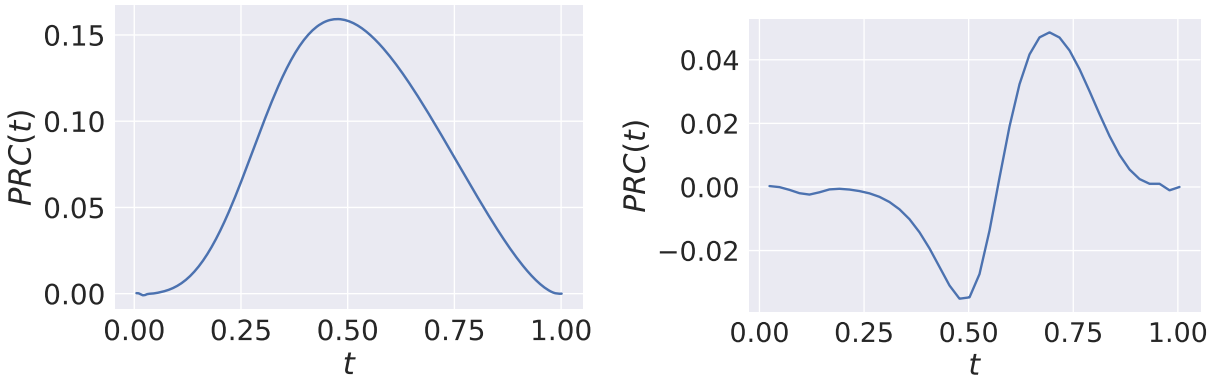

Figure 4.4: PRC calculated using Morris-Lecar equations descriving a single neuron. With Class-I excitability parameters in (a) and Class-II excitability parameters in (b).

This categorization has been proved by Ermentrout to be closely related with the excitability class of the neuron. In [41] is shown that Class-I excitable systems are associated with Type-I PRC and that Class-II excitable systems are associated with Type-II PRC.

Following this direction, theoretical results [41],[42] suggest that Type-II excitable membranes are more likely to synchronize than Type-I membranes. However, it is unknown how many shapes of PRCs can be found and if they have similar effects. Here, we calculate the PRC for the Neural Mass model, and shown the results in Fig. 4.5.

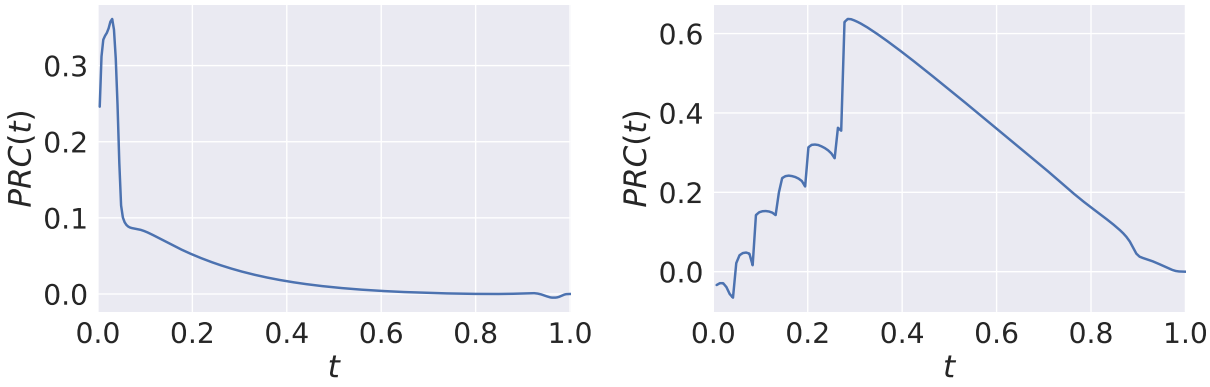

a) b)

Figure 4.5: PRC calculated using Larter Breakspear equations describing a single neuron. Using Class-I excitability parameters in (a) and Class-II excitability parameters in (b).

Similar results for Homoclinic bifurcation were shown in [43]. Interestingly, our results agree with [42] as the case of the Subcritical Hopf bifurcation displaying Class-II excitability does indeed synchronize. However, we cannot disregard the large difference between both Class-II excitability PRCs between the Morris-Lecar and the Larter-Breakspear model. In Fig 4.4 (b) one can see a large enough region of negative PRC while in Fig 4.5 (b) this region is relatively small and may resemble more to a Type-I PRC.

The synchronization between two NMs simulated using Larter-Breakspear model is justified as the system has a negative transverse Lyapunov exponent. This was reported to depend on the coupling strength, C. It is when the coupling becames too weak, that the transverse Lyapunov exponent changes from negative to positive, and the coupled system displays then chaotic behavior [25].

Chapter 5

Finding Anticipated Synchronization

More than a decade ago, Voss reported a new scheme of synchronization [44] that he called Anticipated Synchronization (AS). He studied two unidirectionally coupled identical systems such as in Fig. 5.1, where the receiver or slave (S) was subject to a negative delayed self-feedback loop.

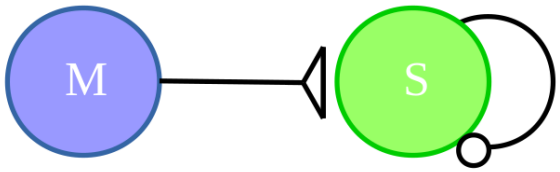

Figure 5.1: Scheme of a unidirectional excitatory coupling between two different NMs. M stands for the Master and S for the slave NM. Slave NM has now an inhibitory self-feedback loop.

In [20], an inhibitory interneuron has been proposed as a biological mechanism for this feedback loop. Following the same way of thinking we can use the Larter-Breakspear model. However, we need to consider now that each NM already has its negative self-feedback loop provided by the inhibitory neurons. So when we couple two of them we will vary the strength of the coupling with the inhibitory interneurons, a_{ie} in order to search the AS regime.

In Fig 5.2 (a) and (b) we plot the histogram of the time distribution between two consecutive spikes for different values of a_{ie}. There we see that for $2.0 < a_{ie} < 2.6$ AS is stable. We can

observe in the traces presented a clear transition from DS to AS, Fig. 5.2 (c),(d) and (e). A longer trace of time of the membrane potential is shown in Fig 5.2 (d).

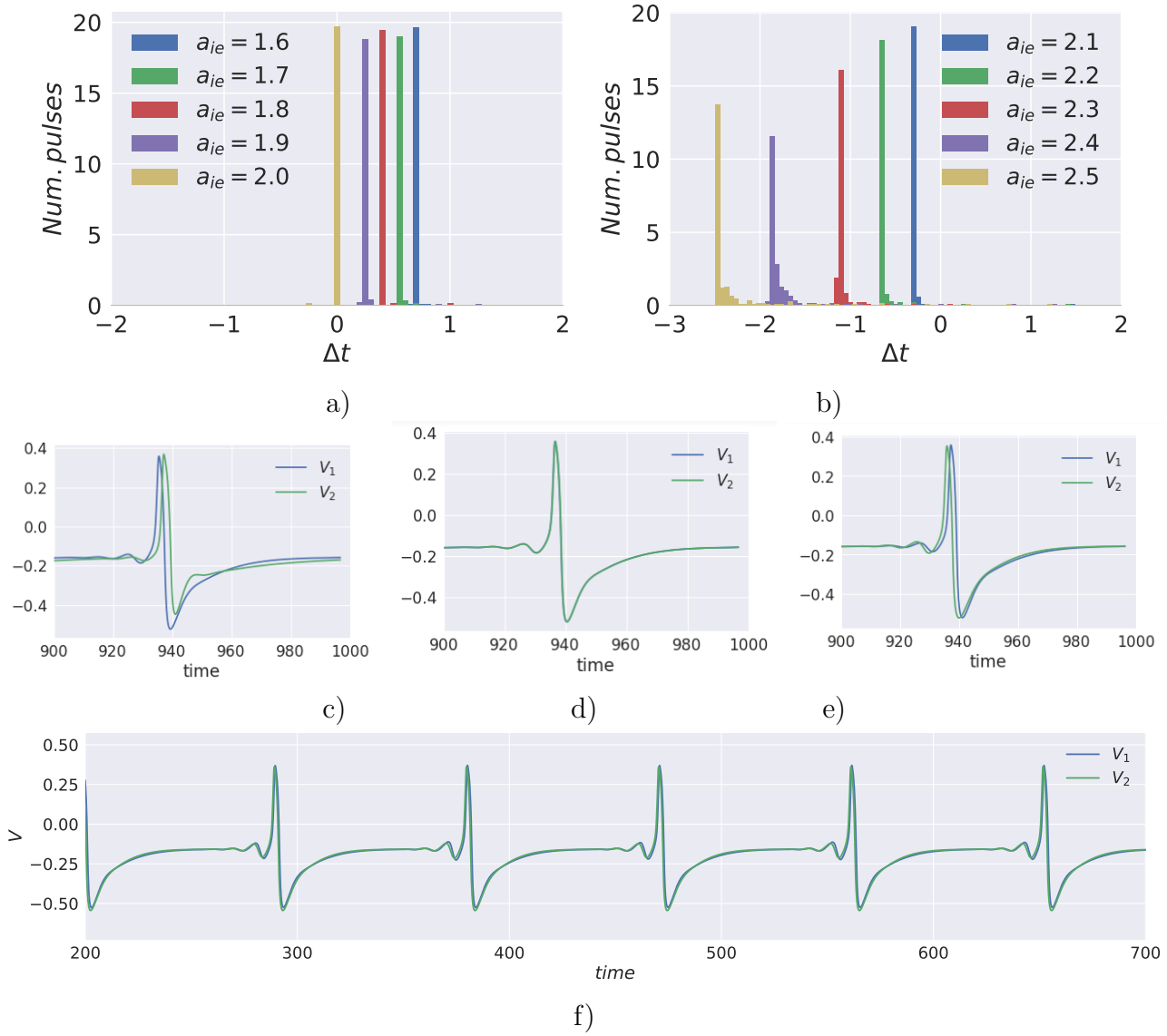

Figure 5.2: Histograms of the time distribution, computed in 20 different trials starting with random initial conditions, for different values of a_{ie} is plotted in (a): we can see direct synchronization and in (b) the transition to AS. Traces corresponding to different values of the internal connectivity strength $a_{ie} = 1.6$, $a_{ie} = 2.3$ and $a_{ie} = 2.6$ are shown in this order in (c),(d) and (e) with $C_{12} = 0.2$. An example of a long trajectory with $a_{ie} = 2.3$ and $C_{12} = 0.2$ is shown in (f).

We also studied the case where the NMs had a slightly different variance for the excitatory threshold, δ_V. Results were robust against this change and one can still observe the same phenomenon. The average value of the time between spikes versus the internal connectivity a_{ie} is plotted in Fig 5.4 (a).

In the brain, most connections are bidirectional, implying that the case studied previously could be too simple to actually justify any observed process.

Thus, we proceed analyzing the case with bidirectional coupling, drawn scheme in Fig. 5.3 (a). In this case, we could also observe AS. However, the maximum anticipated time observed between the slave and the master diminishes compared to unidirectional coupling. The histogram of the time distribution between spikes is plotted in Fig. 5.4 (a) and (b), in Fig. 5.5 (b) one can find the dependence of the average time between spikes with the internal connectivity a_{ie}.

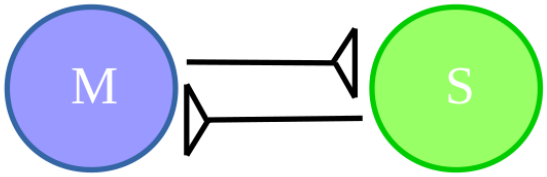

Figure 5.3: Scheme of a bidirectional excitatory coupling between two different NM. M stands for the Master and S for the slave NM.

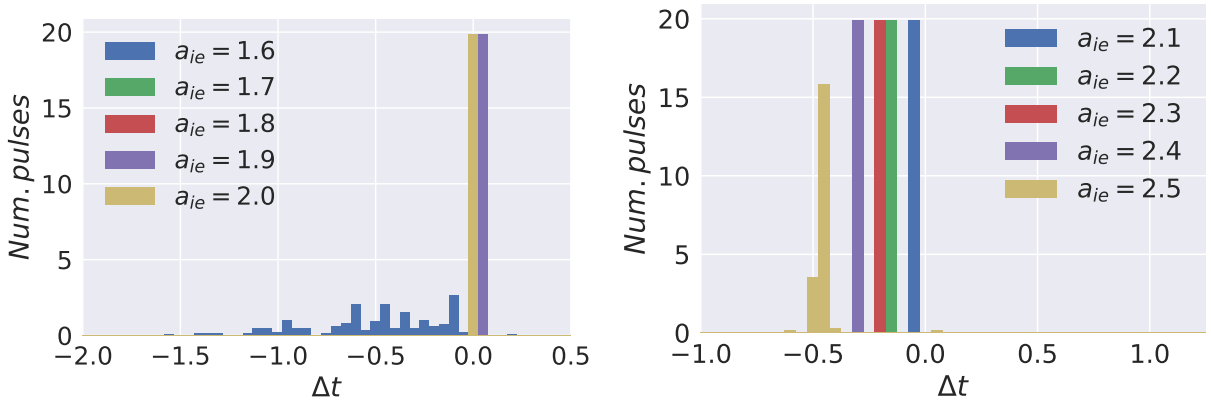

a) b)

Figure 5.4: Histogram of the time distribution, computed in 20 different trials starting with random initial conditions, for different values of a_{ie} considering the scheme of bidirectional coupling with $C_{12} = C_{21} = 0.2$ is plotted in (a), where we can see direct synchronization. Distributions for $1.7 < a_{ie} < 1.9$ are centered in the same bin. In (b) the transition to AS.

We did not observe for the moment that variations in frequency or other internal connectivity strengths could lead to the same AS behavior. We do analyze also if the change in the external intensity input could have some implications in how the master and slave system synchronize. This also gives a regime of AS although only for a very narrow range of values. Fig 5.5 (c) shows how the average value of time between spikes depending on the intensity applied in the slave NM.

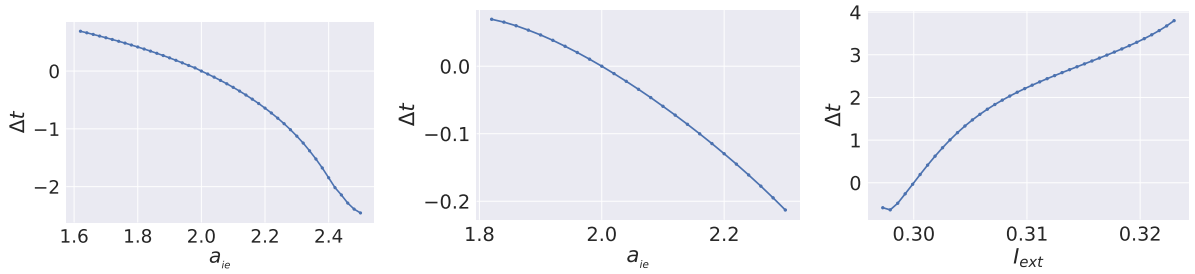

a) b) c)

Figure 5.5: Comparison of the average time between master and slave spikes in the different situations considered. A transition from DS to AS varying a_{ie} for directional coupling between NMs is shown in (a) and the one with bidirectional coupling in (b). Transition due to the variation of the external intensity applied to the slave NM is shown in (c). Value for the coupling constant between NMs in (a) and (c) is $C_{12} = 0.2$ and $C_{21} = 0.0$, in (b) $C_{12} = C_{21} = 0.2$

Chapter 6

Conclusion

6.1 Summary of Thesis Achievements

In this master thesis we reproduced some results previously presented in literature concerning synchronization in Larter-Breakspear model. We have continued testing further the model to understand what kind of behaviors can display and arrived to some remarkable results.

We have also studied the AS regime and found that it is stable for some parameter values. This has helped us gain insight into the mechanisms that could lead to this behavior reported in previous experiments and to understand the importance of feedback-loops, circuitry and complex dynamics in the brain.

Although, different variations in the model parameters make the system display AS, we are still not sure if there are more possible situations that could lead to the same behavior. We also do not know if it is only a change in the inhibitory conductance or the intensity applied that are causing AS in the brain or it is a combination of these or more mechanisms that ends up displaying this behavior. In order to solve all those new questions that arise further work is needed.

6.2 Future Work

Natural lines to extend this project could go through the addition of noise in order to test the robustness of the model. Also, comparison with real data to see if this mechanism is enough to justify the behavior observed in the brain could consolidate the mechanisms proposed.

On the other hand, obtaining the bifurcation diagram in order to study how the model behaves near other type of bifurcations could be interesting. For example close to a SNIC, it would be interesting to see if the system has a stable regime of synchronization. This is related to the following point, where a better understanding of PRC functions and how they can be related with synchronization and excitability is needed. Maybe taking into account different shapes or trying to verify those experimentally. This direction has been followed by other groups in [45].

Trying to reproduce a more complex spatial mapping of some regions of the scalp could be an interesting point. In order to see if the topology underneath or the heterogeneity of other NM could disseminate the synchronization observed. Similar results have been found in literature when studying neural networks analyzed in [46].

Other direction could be trying to build a less simplistic connectivity scheme for a NM. Trying to implement a more involved circuitry reported in the cortical column as has been studied for example in [47]. It would be interesting also to understand the implications that AS could have concerning Hebbian rules and learning processes in the brain.

Appendix

Table 1: Parameter values and its description for the Morris-Lecar.

Parameter	Description	Value
$v_{_{Ca}}$	Calcium equilibrium potential	1
$v_{_K}$	Potassium equilibrium potential	-0.7
$v_{_L}$	Leak equilibrium potential	-0.5
$g_{_K}$	Potassium ionic conductance	2
$g_{_L}$	Leak ionic conductance	0.5
ϕ	Potassium rate constant	1/3
V_1	Calcium activation potential	-0.01
V_2	Calcium reciprocal slope	0.15
V_3	Potassium activation potential	0.1
V_4	Potassium reciprocal slope	0.145

Table 2: Parameter values and its description for the Morris-Lecar model for the case of Class-II excitability and Class-I exctiability.

Parameter	Description	Type I value	Type II value
g_{Ca}	Calcium ionic conductance	1	0.5
I_{ext}	Applied current	0.09	0.15

Table 3: Parameter values and it description for the Larter Breakspear model [30]

Parameter	Description	Value
T_{Ca}	Threshold value for Ca	-0.01
δ_{Ca}	Variance of Ca channel threshold	0.15
g_{Ca}	Conductance of population of Ca channels	1.1
V_{Ca}	Ca Nernst potential	1.0
T_{K}	Threshold value for K	0.0
δ_{K}	Variance of K channel threshold	0.3
g_{K}	Conductance of population of K channels	2.0
V_{K}	K Nernst potential	-0.7
T_{Na}	Threshold value for Na	0.3
δ_{Na}	Variance of Na channel threshold	0.15
g_{Na}	Conductance of population of Na channels	6.7
V_{Na}	Na Nernst potential	0.53
g_{L}	Conductance of population of leak channels	-0.5
V_{L}	Nernst potential of Leak channels	0.5
V_{T}	Threshold potential for excitatory neurons	0.0
δ_{V}	Variance of excitatory threshold	Varied
Z_{T}	Threshold potential for inhibitory neurons	0.0
δ_{Z}	Variance of inhibitory threshold	0.7
I_{ext}	Subcortical input strength	0.3
a_{ee}	Excitatory-to-excitatory synaptic strength	0.4
a_{ei}	Excitatory-to-inhibitory synaptic strength	2.0
a_{ie}	Inhibitory-to-excitatory synaptic strength	2.0
a_{ne}	Non-specific-to-excitatory synaptic strength	1.0
a_{ni}	Non-specific-to-inhibitory synaptic strength	0.4
b	Time constant scaling factor	0.1
ϕ	Time constant scaling factor	0.7
τ	Temperature scaling factor	1.0
r_{NMDA}	Time constant for K scaling factor	0.25

Bibliography

[1] Friston, Karl J. *Functional and effective connectivity in neuroimaging: a syntesis.* Human brain mapping 2.1-2 (1994): 56-78.

[2] Bettencourt, Luis MA, et al. *Functional structure of cortical neuronal networks grown in vitro.* Physical Review E 75.2 (2007): 021915.

[3] Bullmore, Ed and Olaf Sporns. *Complex brain networks: graph theoretical analysis of structural and functional systems.* Nature reviews. Neuroscience 10.3 (2009): 186.

[4] Eytan, Danny and Shimon Marom. *Dynamics and effective topology underlying synchronization in networks of cortical neurons.* Journal of Neuroscience 26.33 (2006): 8465-8476.

[5] Abarbanel, H. D. I., et al. *Synchronisation in neural networks.* Physics-Uspekhi 39.4 (1996): 337-362.

[6] Beggs, J. M. and Plenz, D. *Neuronal Avalanches in Neocortical Circuits.* Journal of Neuroscience 23(35), 11167-11177,2003.

[7] Song, S., Miller, K. D. and Abbott, L. F. *Competitive Hebbian learning through spike-timing-dependent synaptic plasticity.* Nature neuroscience, 3(9), 919-926, 2000.

[8] Bi, G. Q. and Poo, M. M. *Synaptic modifications in cultured hippocampal neurons: Dependence on spike timing, synaptic strength, and postsynaptic cell type* Journal of neuroscience, 18(24), 10464-10472, 1998.

[9] Mirasso, C. R., Colet, P., and García-Fernández, P. *Synchronization of chaotic semiconductor lasers: Application to encoded communications.* IEEE Photonics Technology Letters, 8(2), 299-301, 1996.

[10] Roy, R., and Thornburg Jr, K. S. *Experimental synchronization of chaotic lasers.* Phys. Rev. Lett. 72(13)(1994), 2009.

[11] Mehta, A. and Barker, G. C. *Disorder, memory and avalanches in sandpiles.* EPL (Europhysics Letters), 27(7), 501. (1994)

[12] Narendra, K. S. *Adaptive and learning systems: theory and applications.* Springer Science and Business Media, 2013.

[13] Singer, Wolf. *Synchronization of cortical activity and its putative role in information processing and learning.* Annual review of physiology 55.1 (1993): 349-374.

[14] Pfurtscheller, Gert, and FH Lopes Da Silva. *Event-related EEG/MEG synchronization and desynchronization: basic principles.* Clinical neurophysiology 110.11 (1999): 1842-1857.

[15] Klimesch, Wolfgang. *Memory processes, brain oscillations and EEG synchronization.* International journal of psychophysiology 24.1 (1996): 61-100.

[16] Liu, Hesheng, et al. *Timing, timing, timing: fast decoding of object information from intracranial field potentials in human visual cortex.* Neuron 62.2 (2009): 281-290.

[17] Matias, Fernanda S., et al. *Modeling positive Granger causality and negative phase lag between cortical areas.* NeuroImage 99 (2014): 411-418.

[18] Locquet, A., C. Masoller, and C. R. Mirasso. *Synchronization regimes of optical-feedback-induced chaos in unidirectionally coupled semiconductor lasers.* Physical Review E 65.5 (2002): 056205.

[19] Masoller, C. *Anticipation in the synchronization of chaotic semiconductor lasers with optical feedback.* Physical Review Letters 86.13 (2001): 2782.

[20] Matias, Fernanda S., et al. *Anticipated synchronization in a biologically plausible model of neuronal motifs.* Physical Review E 84.2 (2011): 021922.

[21] Jansen, Ben H., and Vincent G. Rit. *Electroencephalogram and visual evoked potential generation in a mathematical model of coupled cortical columns.* Biological cybernetics 73.4 (1995): 357-366.

[22] Gollo, Leonardo L., et al. *Mechanisms of zero-lag synchronization in cortical motifs.* PLoS computational biology 10.4 (2014): e1003548.

[23] Spiegler, Andreas, et al. *Complex behavior in a modified Jansen and Rit neural mass model.* BMC Neuroscience 12.1 (2011): P5.

[24] Morris, Catherine, and Harold Lecar. *Voltage oscillations in the barnacle giant muscle fiber.* Biophysical journal 35.1 (1981): 193-213.

[25] Breakspear, Michael, John R. Terry, and Karl J. Friston. *Modulation of excitatory synaptic coupling facilitates synchronization and complex dynamics in a biophysical model of neuronal dynamics.* Network: Computation in Neural Systems 14.4 (2003): 703-732.

[26] Abbott, L.F. *Lapique's introduction of the integrate-and-fire model neuron (1907).* Brain Research Bulletin. 50 (1999): 303-304.

[27] Hodgkin, A. L.; Huxley, A. F. *A quantitative description of membrane current and its application to conduction and excitation in nerve.* The Journal of Physiology. 117 (1952): 500-544.

[28] FitzHugh R. *Mathematical models of threshold phenomena in the nerve membrane.* Bull. Math. Biophysics, 17 (1955): 257-27.

[29] Kobelevskiy I. *Bifurcation analysis of a system of Morris-Lecar neurons with time delayed gap junctional coupling.* MS thesis. University of Waterloo, 2008.

[30] P. Dayan and L.F.Abbot, *Theoretical Neuroscience: Computational and Mathematical Modeling of Neural Systems.* MIT Press, 2001.

[31] David O., Kiebel S., Harrison L., Mattout J., Kilner J., Friston K. *Dynamic causal modeling of evoked responses in EEG and MEG.* Neuroimage 30, (2006): 1255-1272.

[32] Lyes Bachatene, Vishal Bharmauria and Stéphane Molotchnikoff. *Adaptation and Neuronal Network in Visual Cortex, Visual Cortex - Current Status and Perspectives* (2012) Available from: https://www.intechopen.com/books/visual-cortex-current-status-and-perspectives/adaptation-and-neuronal-network-in-visual-cortex

[33] Ranson, Stephen Walter, and Sam Lillard Clark. *The Anatomy of the Nervous System. Its Development and Function.* Academic Medicine 34.5 (1959): 553.

[34] Teplan, Michal. *Fundamentals of EEG measurement.* Measurement science review 2.2 (2002): 1-11.

[35] Larter, Raima, Brent Speelman, and Robert M. Worth. *A coupled ordinary differential equation lattice model for the simulation of epileptic seizures.* Chaos: An Interdisciplinary Journal of Nonlinear Science 9.3 (1999): 795-804.

[36] Deco, Gustavo, et al. *The dynamic brain: from spiking neurons to neural masses and cortical fields.* PLoS computational biology 4.8 (2008): e1000092.

[37] Marreiros, André C., Stefan J. Kiebel, and Karl J. Friston. *A dynamic causal model study of neuronal population dynamics.* Neuroimage 51.1 (2010): 91-101.

[38] Marreiros, André C., et al. *Population dynamics under the Laplace assumption.* Neuroimage 44.3 (2009): 701-714.

[39] Luo, Albert CJ. *A theory for synchronization of dynamical systems.* Communications in Nonlinear Science and Numerical Simulation 14.5 (2009): 1901-1951.

[40] Stepanyants, Armen, et al. *The fractions of short-and long-range connections in the visual cortex.* Proceedings of the National Academy of Sciences 106.9 (2009): 3555-3560.

[41] Ermentrout, Bard. *Type I membranes, phase resetting curves, and synchrony.* Neural computation 8.5 (1996): 979-1001.

[42] Abouzeid, Aushra, and Bard Ermentrout. *Type-II phase resetting curve is optimal for stochastic synchrony.* Physical Review E 80.1 (2009): 011911.

[43] Brown, Eric, Jeff Moehlis, and Philip Holmes. *On the phase reduction and response dynamics of neural oscillator populations.* Neural computation 16.4 (2004): 673-715.

[44] Voss, Henning U. *Anticipating chaotic synchronization.* Physical review E 61.5 (2000): 5115.

[45] Galán, Roberto F., G. Bard Ermentrout, and Nathaniel N. Urban. *Efficient estimation of phase-resetting curves in real neurons and its significance for neural-network modeling.* Physical review letters 94.15 (2005): 158101.

[46] Motter, Adilson E., Changsong Zhou, and Jurgen Kurths. *Network synchronization, diffusion, and the paradox of heterogeneity.* Physical Review E 71.1 (2005): 016116.

[47] Grossberg, Stephen, Ennio Mingolla, and William D. Ross. *Visual brain and visual perception: How does the cortex do perceptual grouping?.* Trends in neurosciences 20.3 (1997): 106-111.